Hindawi Publishing Corporation
X-Ray Optics and Instrumentation
Volume 2010, Article ID 867049, 17 pages
doi:10.1155/2010/867049

Review Article

Focusing Polycapillary Optics and Their Applications

Carolyn A. MacDonald

Center for X-Ray Optics, University at Albany, SUNY, Albany, NY 12222, USA

Correspondence should be addressed to Carolyn A. MacDonald, c.macdonald@albany.edu

Received 23 April 2010; Revised 26 August 2010; Accepted 18 October 2010

Academic Editor: Ali Khounsary

A summary of focusing X ray polycapillary optics is presented including history, theory, modeling, and applications development. The focusing effects of polycapillary optics come from the overlap of the beams from thousands of small hollow glass tubes. Modeling efforts accurately describe optics performance to allow for system development in a wide variety of geometries. The focusing of X ray beams with polycapillary optics yields high gains in intensity and increased spatial resolution for a variety of clinical, lab-based, synchrotron or in situ analysis applications.

1. Introduction

Polycapillary optics are arrays of small hollow glass tubes. X rays are guided down these curved and tapered tubes by multiple reflections in a manner analogous to the way fiber optics guide light. They differ from single-bore capillaries and X ray mirrors in that the focusing or collecting effects come from the overlap of the beams from thousands of channels, rather than from a few surfaces. Generally, this results in relatively efficient collection, especially from large divergent sources such as conventional X ray tubes, but does not produce submicron beam spot sizes.

The potential for guiding X rays down single-capillary tubes by total reflection was noted in the 1950s [1, 2] and measured in the 1960s [3] and 70s [4–6]. The invention of polycapillary optics by Kumakhov was built on this work [7–10] and inspiration from ion channeling and channeling radiation [11]. A theoretical review of the potential for polycapillary optics and prototype testing was published in 1990 [12].

In November of 1990, the Center for X Ray Optics (CXO) at the University at Albany was jointly founded with the Institute for Roentgen Optical Systems (IROS) in Moscow as part of an agreement between Kumakhov and the late Gibson to jointly develop the technology [13–15] both at these institutes and at a jointly founded company, X Ray Optical Systems (XOS). Early work at CXO [16–21] and IROS [22–25] was concerned with developing techniques for systematic measurements and of investigating the potential for application development. In 2001, Gibson retired from the university and moved to XOS. Kumakhov also worked in commercialization of the optics with other companies, especially with Unisantis. Over the years, many more groups have contributed to the worldwide development of the optics. Not every group can be mentioned here, but more than two dozen are cited in this paper. In addition, while in the discussion of the behavior of the optics, example data has largely been drawn from CXO, in many cases similar data could have been obtained from almost any of the other groups.

Polycapillary optics are well suited for clinical, *in situ*, or laboratory-based applications such as X ray fluorescence and X ray diffraction, especially on small samples [26, 27]. Because they are based on reflection, not diffraction, they are achromatic, appropriate for broadband applications, including white beam synchrotron focusing and collection of astronomical signals for spectroscopy.

X rays can be transmitted down a curved hollow tube as long as the tube is small enough, and bent gently enough, to keep the angles of incidence less than the critical angle for total reflection, θ_c. The critical angle for borosilicate glass is approximately

$$\theta_c \approx \frac{30\,\text{keV}}{E}\,\text{mrad}, \tag{1}$$

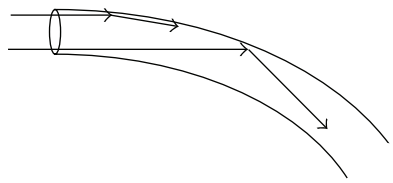

Figure 1: X rays traveling in a bent capillary tube. The trajectory of the ray entering at the top at grazing incidence is projected onto the page, but in three dimensions will "toboggan" in a constant radius spiral. The X ray entering at the bottom (closest to the center of curvature) strikes at a larger angle.

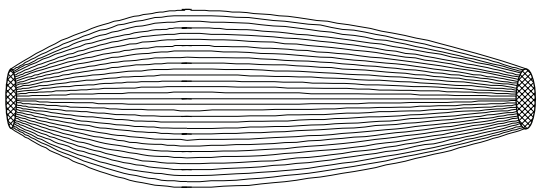

Figure 2: Sketch of the interior channels of a monolithic polycapillary optic with a short input and longer output focal length.

which is approximately 1.7° for 1 keV photons and 0.086° for 20 keV photons. The angles are somewhat larger for leaded glass.

As shown in Figure 1, the angle of incidence for rays entering a bent tube increases with tube diameter. The requirement that the incident angles remain less than the critical angle necessitates the use of small channel sizes, typically between 2 and 50 μm, although research for submicron channel sizes is reported in Section 5.6. The optics are produced by pulling large diameter glass tubes to create small diameter tubes, stacking and pulling them together, and repeating. The final pull is designed to create a section with the desired shape, from which the ends are cut away, as shown in Figure 2.

2. Alignment and Transmission with Tube Sources

Standard techniques have been developed for aligning and characterizing polycapillary optics with tube sources [17–19, 24, 28–30]. The optic is typically first rough aligned by determining the location and direction of the most intense part of the X ray cone emitted from the tube source. This can be accomplished by placing two washers in the path, as shown in Figure 3. The first washer is translated until the image of the washer is centered in the most intense part of the beam. The second washer is then translated until the two images are concentric, as shown in Figure 4. Lasers can then be aligned to the two washers to provide a rough beam axis.

To begin alignment, the optic is placed near the source, as shown in Figure 5. Then, depending on the source geometry, either the source or the optic is translated in the two dimensions perpendicular to the optic axis in small steps, producing a measurement of intensity versus relative source position, as shown in Figure 6 [29]. Alternatively, the optic

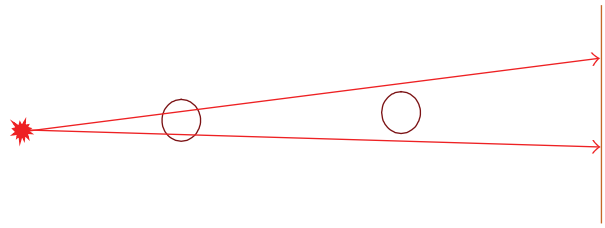

Figure 3: Alignment of washers.

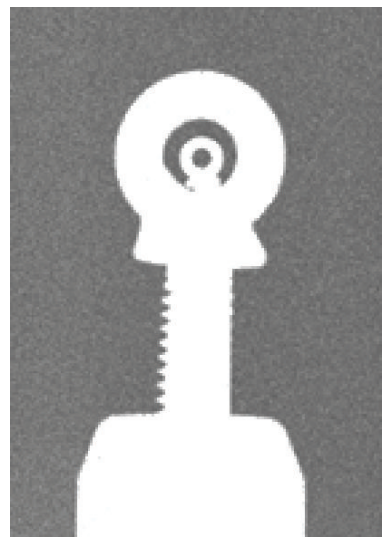

Figure 4: Image of two washers of the same size [31].

may be rotated in two dimensions [28]. In order to determine the focal length of the optic, scans are repeated at increasing distances from the source. When the source is away from the focal point, the intensity is low and the scan is broad. Near the focal point, the plots are symmetric and Gaussian, which indicates good alignment of the source, optic, and detector. At the focal distance, the ratio of the width of the scan curve to the optic-to-source distance, called the source scan angle,

$$\varepsilon = \frac{\Delta x}{z}, \tag{2}$$

should be a minimum, as shown in Figure 7. At the focal point, the maximum source size that is captured by the optic is approximately

$$\mathrm{D}_{\mathrm{source}} \sim f\ \theta_c, \tag{3}$$

where f is the input focal length of the optic and θ_c is the critical angle for reflection. Rays originating from outside this range are incident on the optic channels at too high an angle to be reflected. Smaller sources allow for smaller input focal lengths and hence higher beam intensity.

Transmission is the ratio of the number of photons passing along the channels to the number incident on the front face of the optic. Transmission with respect to the source-optic distance is also shown in Figure 7. The highest transmission and the lowest source angle occur at

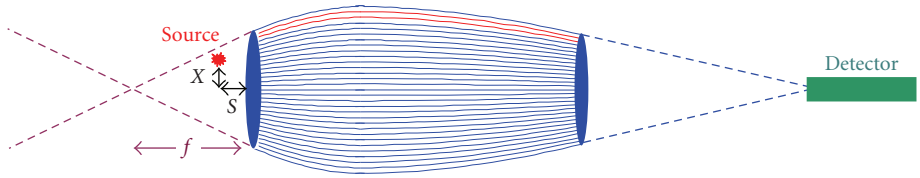

Figure 5: Geometry for source scans. With the source at a distance S which is less than the input focal length f, only a few channels of the optic transmit.

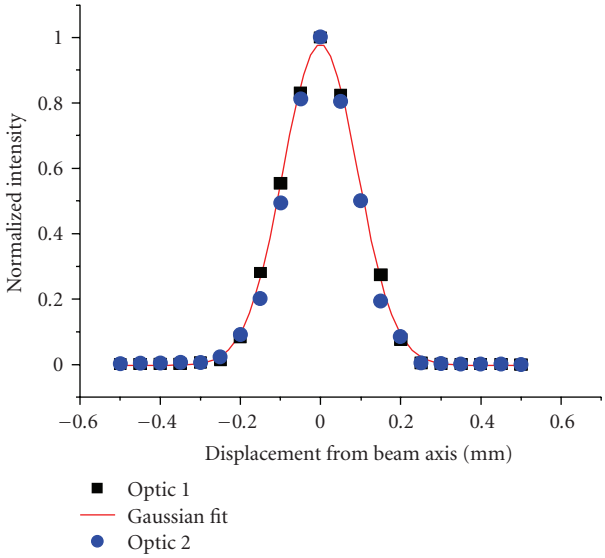

Figure 6: Source scan with the source near the focal point, taken at 17.5 keV for two different optics with input focal lengths ranging from 48–56 mm.

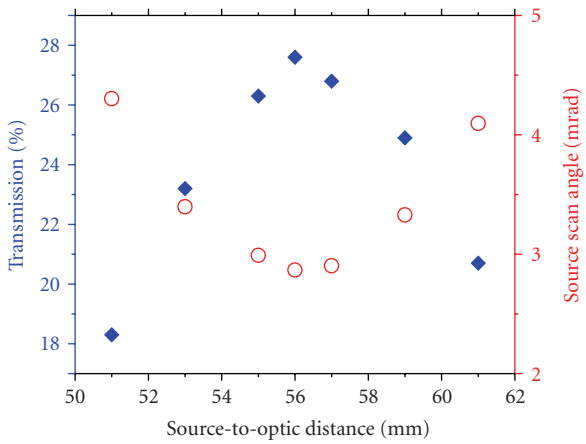

Figure 7: Transmission (♦) and source angle (O) versus source distance. The transmission is the highest at the design focal length of 56 mm.

the focal distance. Transmission at the focal distance as a function of photon energy can be measured with an energy sensitive detector, with a typical result shown in Figure 8. The transmission falls with photon energy because of the energy dependence of the critical angle given in (1). The maximum

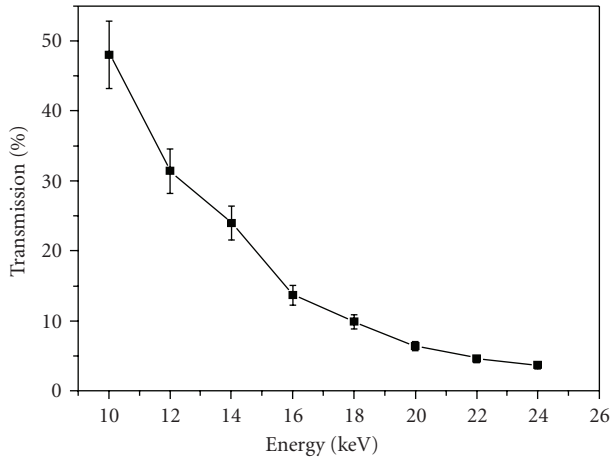

Figure 8: Transmission versus energy for a focusing optic with a 58 mm input focal length and 119 mm output focal length.

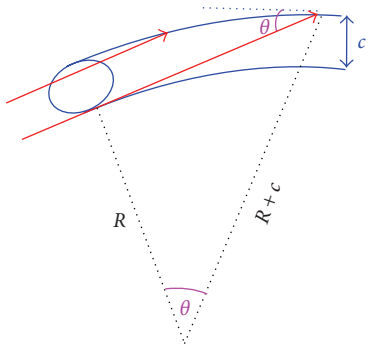

Figure 9: Estimating the maximum incident angle, θ.

incident angle for a input beam can be estimated from the channel size and bending radius, as shown in Figure 9, using

$$\cos(\theta) = \frac{R}{R+c} \Longrightarrow 1 - \frac{\theta^2}{2} \approx \frac{1}{1+(c/R)} \approx 1 - \frac{c}{R} \Longrightarrow \theta \approx \sqrt{\frac{2c}{R}}, \tag{4}$$

where R is the radius of curvature of the channel and c is the channel diameter. R can be estimated from the length of the optic as in Figure 10 by

$$L \approx 2\frac{R}{2}\phi \Longrightarrow R \approx \frac{L}{\phi}, \tag{5}$$

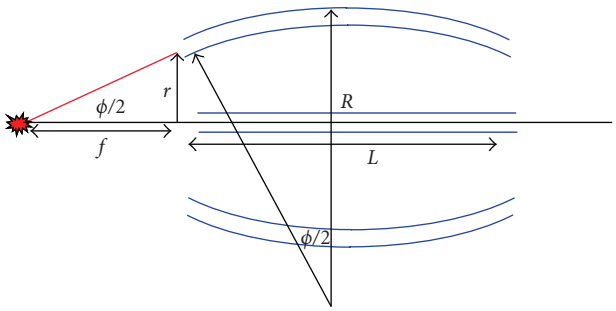

Figure 10: Estimation of channel bending radius, R.

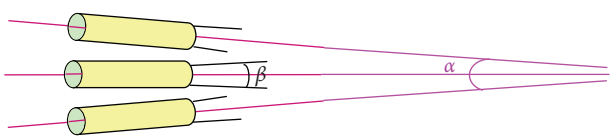

Figure 11: Global divergence, α.

where L is the length of the optic and ϕ is the capture angle, found from the radius of the optic, r, and the focal length, f,

$$\phi = 2\,\mathrm{atan}\left(\frac{r}{f}\right). \tag{6}$$

For the optic measured in Figure 8, $c = 10\,\mu$m, and $R \approx 2.7$ m, giving a maximum incident angle of 2.7 mrad, equal to the critical angle for 11 keV photons. At 10 keV, the transmission is 50%, nearly the full fraction of the front face not filled by glass walls, but the transmission drops rapidly with energy as the critical angle decreases below the maximum incident angle.

3. Divergence and Focal Spot Size

As shown in Figure 11, the output from a polycapillary focusing optic has both global divergence, α, and local divergence, β. Even for a collimating optic, where the channels are parallel on output ($\alpha = 0$), the output divergence, β, is not zero, but is approximately given by the critical angle and therefore is dependent on the X ray energy [32]. The local divergence and transmission losses will result in a beam spot which is less intense than the emission spot on the anode. This is consistent with the second law of thermodynamics, which requires that the photon state density in phase space cannot increase, as sketched in Figure 12.

The total divergence, $\alpha + \beta$, at a energy of a Bragg peak can be estimated by rotating a high quality crystal in the beam and measuring the angular width of the peak, as shown in Figure 13 [33]. The inherent width of the Bragg peak is typically a few eV [34, 35], so that the angular width, given by Bragg's law, is

$$\Delta\theta = -\tan\theta\frac{\Delta E}{E} \tag{7}$$

usually less than 100 μrad. Since the Darwin width and mosaicity of the crystal are typically also much smaller

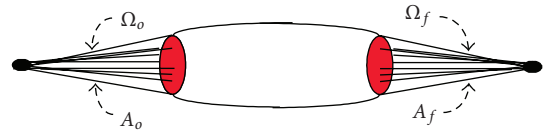

Figure 12: Liouville's Theorem requires that $A_o\Omega_o \le A_f\Omega_f$ for each photon energy transmitted by any optic.

than the exit divergence from the optic, the measurement yields the divergence directly. Using collimating optics, the local divergence, β, has been measured and typically is $\sim 1.3\theta_c$. The factor 1.3 is an experimentally determined parameter that arises from the fact that most of the beam has a divergence less than the maximum divergence of $2\theta_c$ produced by reflection at the critical angle. Unlike the case for pinhole collimation, the local divergence of the beam does not depend on the source size, although it should be remembered, as noted in (3), that large sources may not be efficiently captured by the optic.

The global divergence can be found separately from the slope of a plot of the beam size versus distance from the optic, as shown in Figure 14. In that instance, an imaging detector was used. However, near the focal point, the spot size can be small compared to the resolution of the imaging detector. The spot can be measured using a knife edge technique as shown in Figures 15, 16, and 17, or by scanning a small pinhole across the beam. Better accuracy in determining the focal spot size requires insuring that the knife edge or detector plane is perpendicular to the beam axis [30].

Assuming perfect overlap, the spot size at the focal point is determined by the spot size from each individual capillary channel, which depends on channel size, c, output focal length, f, and local divergence, β, as shown in Figure 18, as

$$d_{\mathrm{spot}} \approx \sqrt{c^2 + (f_{\mathrm{out}} \cdot \beta)^2}. \tag{8}$$

The critical angle, θ_c, at 20 keV is 1.5 mrad. Using $\beta \sim 1.3\theta_c$, an optic with $c = 3.4\,\mu$m and $f_{\mathrm{out}} = 9$ mm has a predicted spot size of 18 μm. An intensity distribution measurement, by the pinhole technique, gave an FWHM of 21 μm [37]. Because of the divergence from each channel, optics with smaller focal lengths have smaller spot sizes, as do measurements at higher photon energies.

Focusing the beam increases the intensity, for example, onto a small sample, compared to pinhole collimation. While for some systems higher intensity could be achieved by simply moving the sample closer to the source, there are generally geometric constraints which limit the minimum distance. If a comparison is made between a pinhole with a diameter σ constrained to be at a distance L from a conventional source, and an optic with focal spot size σ focused at the pinhole location L, the gain is given by

$$\mathrm{Gain} = \left(\frac{d_{\mathrm{optic}}^2}{f_{\mathrm{in}}^2}\right) T \left(\frac{L}{\sigma}\right)^2, \tag{9}$$

where d_{optic} is input diameter of the optic, T is the transmission, and f_{in} is the input focal length. Measured gains are in good agreement with this computation [32].

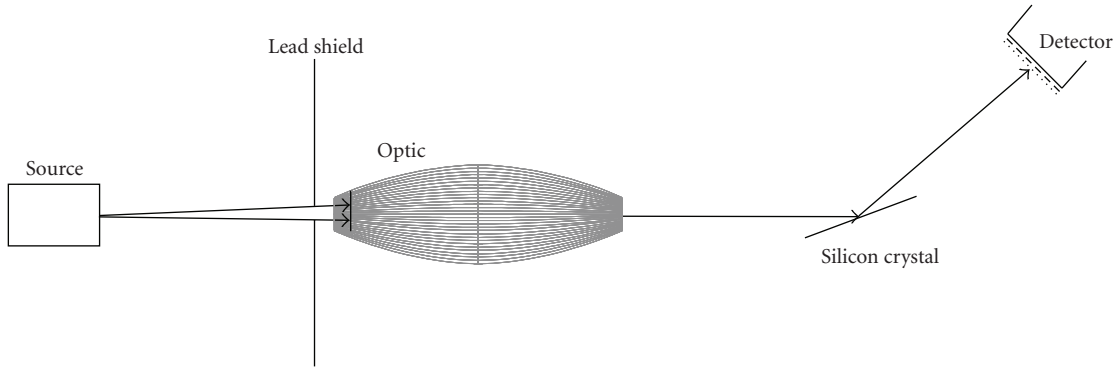

Figure 13: Rocking curve geometry for focusing optic.

Table 1: Results for monolithic focusing optic in a synchrotron beam [38]. The spot size was measured using the knife edge technique. The gain was calculated as for (9) taking $f_{in} \sim L$, given the low divergence of the synchrotron beam.

X ray energy (keV)	Spot size (mm)	Transmission (%)	Measured Gain 350 μm pinhole	Calculated Gain 350 μm pinhole
6	0.09	36	78	81
8	0.08	49	96	110
10	0.09	39	83	87
12	0.09	39	74	87
white	0.17	42	11	89

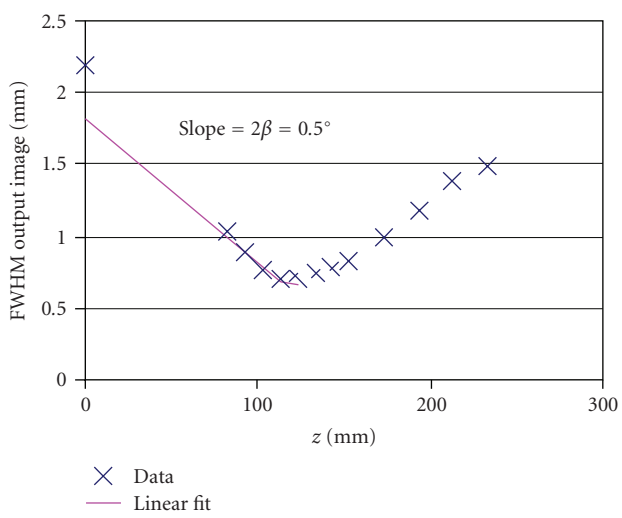

Figure 14: Global divergence of focusing optic found by a linear fit to the beam size on an imaging detector versus optic-to-detector distance [33].

Similarly, polycapillary optics can be used to focus synchrotron beams. For example, Table 1 shows the result of focusing white beam bending magnet radiation using a 5 mm diameter optic with a 17 mm focal length. The measured gain for a 350 μm sample was ~100x, and the calculated gain through a 10 μm pinhole for this optic was more than 1000 [38]. Polycapillary optics have been installed on beamlines at BESSY [39], Hasylab [40–42], and ESRF [43], generally for micro X ray Fluorescence (μXRF) but also for a variety of other applications, including spectroscopy. More discussion of applications is included in Section 6.

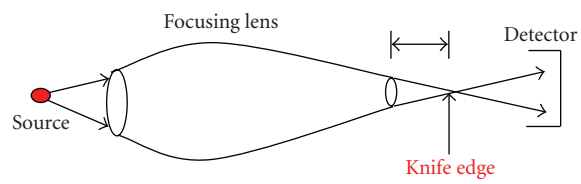

Figure 15: Geometry for knife edge measurement.

4. Energy Filtering

The dependence of the critical angle for reflection on photon energy results in an energy-dependent transmission, as shown in Figure 8. Thus, capillary optics can be used as a low pass filter, using the same principle as for the mirrors commonly used for synchrotron and plasma facilities. With this low pass filter, higher-order harmonics can be removed from the output of a crystal monochromator [44] or from conventional sources for energy-dispersive X ray diffractometry and reflectometry [45]. With the optics, high anode voltages can be used to increase the intensity of the characteristic lines without increasing the high energy background. An example of the effect of a polycapillary optic designed to pass 8 keV Cu $K\alpha$ radiation is shown in Figure 19 [32]. The optic slightly reduces the Cu $K\beta$ 9 keV peak and suppresses the high energy bremsstrahlung. For low resolution diffraction applications, the energy filtration provided by the optic allowed the monochromator to be

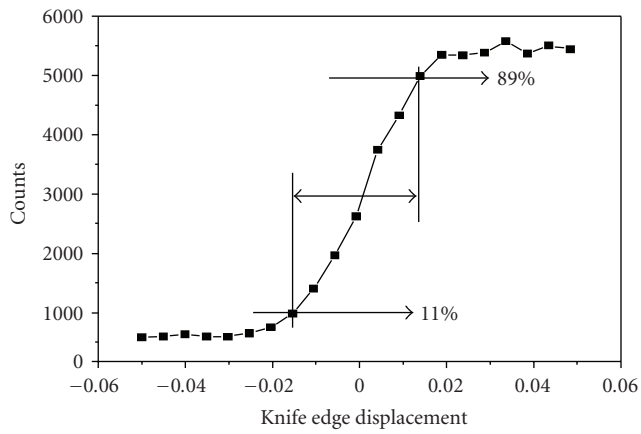

Figure 16: Results of a knife edge measurement. The width can be found by numerical differentiation or by assuming a Gaussian intensity distribution and directly determining the FWHM from the scan. In this case the width was 39 μm [36].

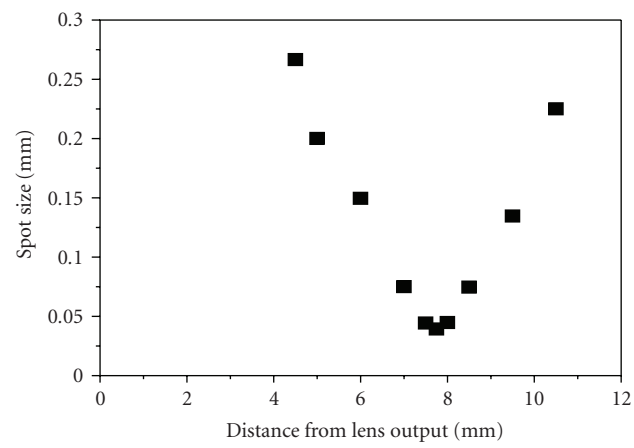

Figure 17: Spot size versus distance from optic.

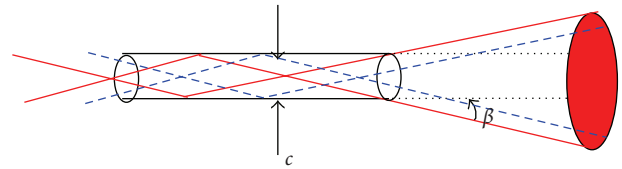

Figure 18: The spot size is enlarged from the channel diameter c because of the local divergence which arises from reflections at angles up to the critical angle.

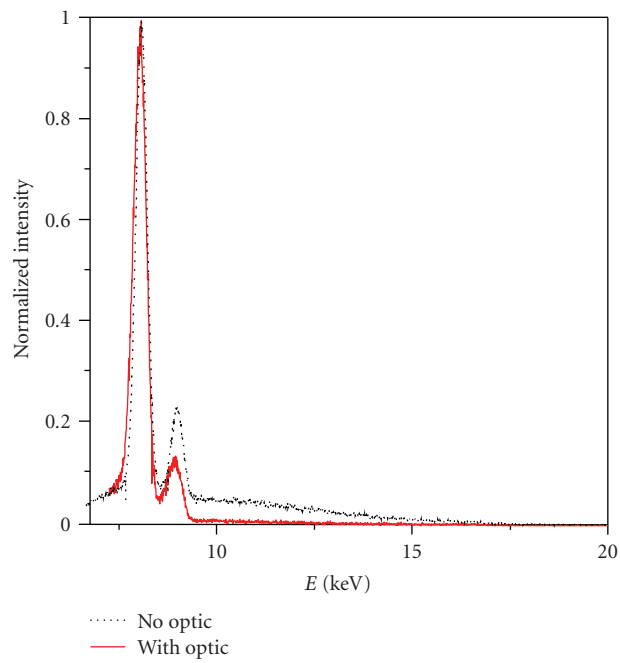

Figure 19: Spectrum of a copper tube source with and without a slightly focusing optic. The optic suppresses the high energy Bremsstrahlung [32].

replaced with a simple nickel absorption filter to remove the $K\beta$ peak.

5. Simulations and Defect Analysis

In order to assess optics defects and also to predict performance in a variety of geometries for applications development, a number of computer codes have been developed to simulate X ray transport in polycapillary optics. Modeling of polycapillary optics requires manipulation of relatively complex geometries compared to one or two bounce mirror optics. Further, because of the multiple reflections, the total throughput, the transmission, is more sensitive to roughness and other optics defects. Early modeling was based on an algorithm developed for ion channeling [46], and included a projection of the three-dimensional geometry onto a moving planar cross-section of the optic channel [17]. Very good agreement was found between simulation and experimental results [47–49] for transmission, absorption, and exit divergence, a wide range of X ray energies, source geometries, and optics lengths, channel sizes, and bend radii.

The realization of numerous applications has been advanced by the development of simulation analyses which allow for increasingly accurate assessment of optics defects. These computer codes, like Shadow [50] are generally based on Monte Carlo simulations of geometrical optics trajectories and provide essential information on performance, design and potential applications of polycapillary optics [51–53]. Generally, a point is selected on the source and the optic face, the ray is propagated until it hits the channel wall surface, a computation is performed of the angle of incidence and hence reflectivity, and the ray, if reflected, is propagated along the channel. If the capillary channel has a complex shape versus distance along the optic axis, the computation of the point of incidence is usually performed by iteration or approximation, and the computation of the surface normal can be complicated.

Some simulations allow for optics defects, discussed below, including roughness, waviness of the capillary walls, channel blockage and profile error to be taken into account.

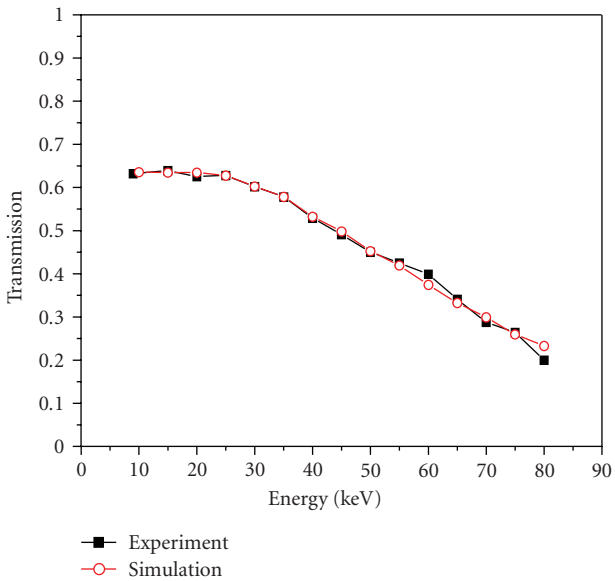

Figure 20: Transmission of a 0.5 mm diameter straight polycapillary optic, compared to a simulation with two fitting parameters, waviness = 0.15 mrad, and unintentional central axis bending radius $R = 120$ m [54]. The fiber had a measured open area of 64.5%, 10 μm channel diameter, and a length of 200 mm.

While characterizing these defects could introduce a large number of fitting parameters, the defects create different signatures in different energy and source geometry regimes, and so can be assessed almost independently. Optics performance over a range of energy from 10 to 80 keV, including multiple datasets of transmission as a function of source position and energy, can often be matched with one or two fitting parameters, as shown in Figures 20 and 21 [55, 56]. For submicron channels, wave effects become significant, as discussed in Section 5.6.

5.1. Open Area. The fractional open area of a polycapillary optic is defined as the fraction of the area of the front face of the optic which is not taken up with the glass walls of the channels. Both the channel diameter and the open area can be measured from microscope images of the front face of the optics. Alternatively, it is simplest to estimate open area for fiber stock by measuring the X ray transmission as a function of energy for short pieces. The transmission maximum is generally equal to the fractional open area.

However, since most optics are sealed to prevent etching by water vapor and avoid other contamination, values of both the channel size and open area must be obtained from the manufacturer. Typical values are 50–70% open area and channel sizes of 5–25 μm. The open area tends to decrease with channel size because of surface tension effects during the drawing of the glass. If it is not known, it can be used as an overall multiplicative fitting parameter independent of photon energy and source location.

5.2. Bending and Profile Error. Bending the channels increases the X ray incidence angles, as shown in Figure 1. Because the critical angle, θ_c, is inversely proportional to the X ray photon energy, bending the channels decreases the X ray transmission down the channels most significantly at higher photon energies. Experimental data taken on a nominally straight fiber (i.e. a thin, straight polycapillary optic) are shown in Figure 22 compared to a CXO simulation [55, 56] which includes otherwise perfect channels with a slight bending. A bending radius smaller than 100 m would underestimate the high energy transmission. Thus the limit on unintentional bending can be estimated solely from the transmission at the highest photon energies. Unintentional bending is consequently unimportant for lower photon energies or channels of an optic which have smaller deliberate bending radii. Simulations with smaller deliberate bending in different shapes also show good agreement to measurements [17].

5.3. Waviness. Midrange spatial frequency slope errors, that is surface oscillations with wavelengths shorter than the capillary length and longer than the wavelength of the roughness, are often called waviness, ripple, or surface oscillations. The detailed shape of the channel walls is unknown, but waviness can be modeled as a random tilt of the glass wall. Waviness is then implemented by changing the surface normal after the point of impact of the ray has been determined. For the CXO simulation, the distribution of surface angles in the glass is assumed to be Gaussian with width w [55, 56]. For high quality glass and photon energies less than 200 keV, w is much smaller than the critical angle, θ_c. Most borosilicate and lead glass optics have simulation fitting parameters which give a Gaussian width for the waviness of 0.12–0.15 mrad. This is in agreement with the directly measured slope variance of the Cornell group [57].

Consideration should be taken in the simulation of the fact that rays are more likely to impact a surface that is tilted toward the ray rather then tilted away [55]. The effect of waviness on fiber transmission is shown in Figure 23. Waviness decreases the transmission a midrange energies, where bending has little effect. The value of the waviness can be estimated from the midrange transmission data alone. Waviness also causes a reduction in the width of source scans at those energies. A simulation fit including waviness and bending for a single 0.5 mm diameter fiber with 10 μm channels is shown in Figure 20 [54].

If the input X ray beam has small local divergence, for example, from a very small spot source, the waviness increases the average angle of reflection and thus the average angle at which X rays exit the fiber. For example, for the case of a small source with a local divergence of 2.4 mrad, a simulation at 8 keV with no channel wall defects produces a divergence less than the critical angle. For a simulation including a typical waviness of 0.15 mrad, the divergence grows to 3.9 mrad, which matches the measured value [56]. In a geometry in which the number of bounces per photon is small, the output divergence can remain smaller than the critical angle.

5.4. Roughness. Roughness is small-scale fluctuations of the glass surface [58, 59]. If the surface can be described as

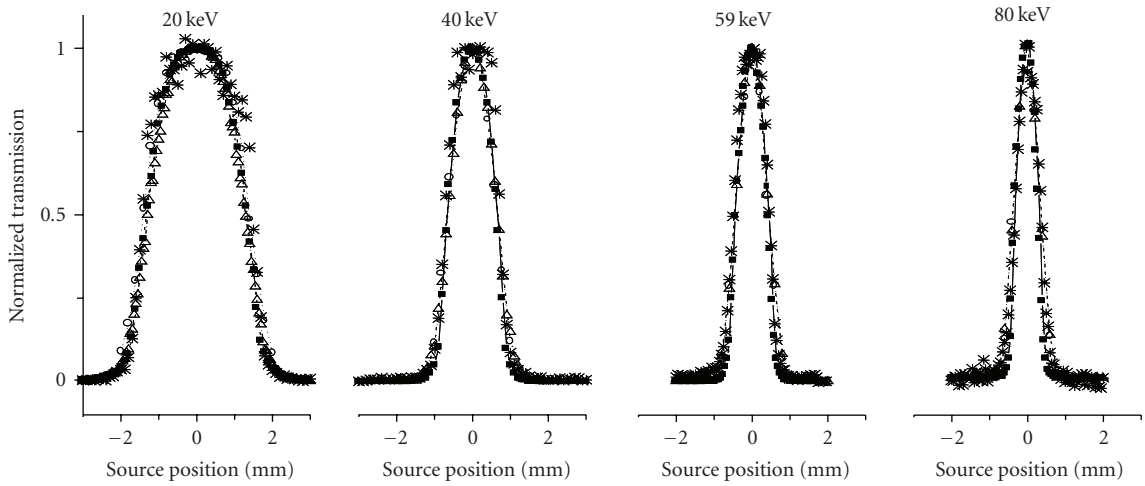

FIGURE 21: Source scan data from the fiber of Figure 20, and simulation (solid line) using the same two fitting parameters, $R = 120$ m, $w = 0.15$ mrad, and also roughness = 0.5 nm.

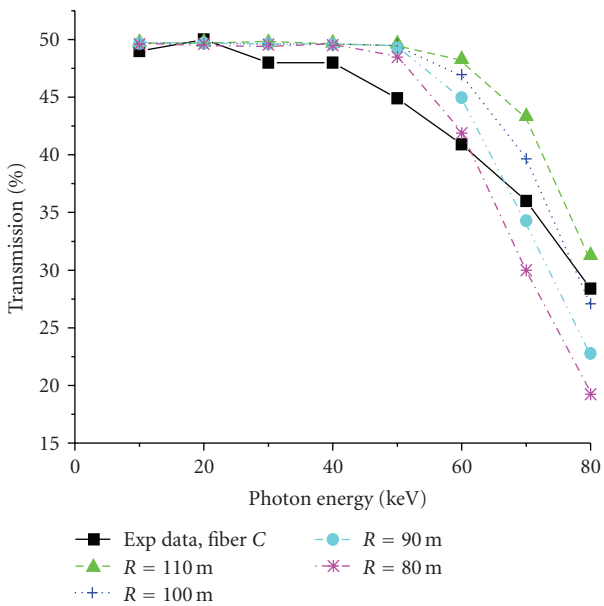

FIGURE 22: Transmission spectra of a thin fiber similar to that of Figure 20, compared to simulations with different bending curvature alone [55]. At the highest energies, a radius of less 100 m will not fit the data. The best fit bending radius will be slightly larger and should be determined after the simulation fitting for waviness is determined.

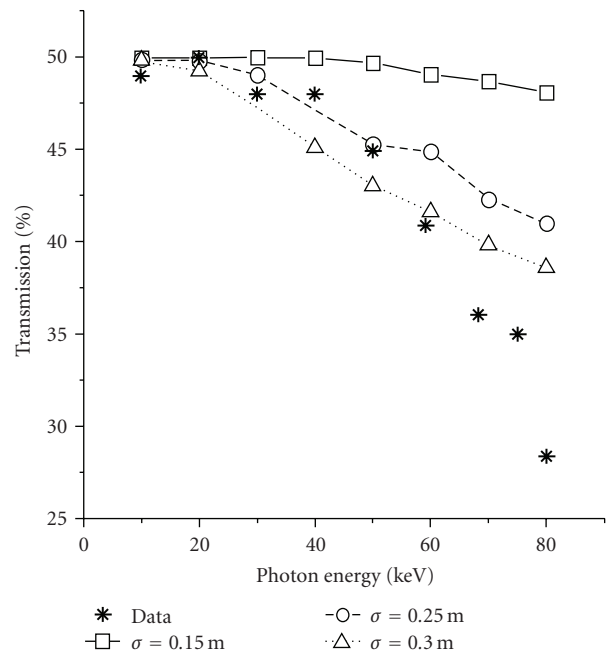

FIGURE 23: Simulations [56] of transmission spectra for a fiber with waviness values from 0.15 to 0.3 mrad compared with the experimental data. A waviness of 0.15 mrad fits the midrange energy data well. That value of waviness should be included with the best fit bending radius [55].

deviating locally from some average smooth surface by an amount $Z(x)$, then the effects are described in terms of roughness correlations which are given in terms of the correlation function $g(x)$,

$$g(x) = \frac{1}{L}\int_0^L Z(x')Z(x'+x)dx' \doteq \overline{Z}^2 e^{-(|x|/s)}, \qquad (10)$$

which has an rms amplitude $\overline{Z}$ and correlation length s. Roughness causes a decrease in reflectivity which depends on both parameters, but becomes relatively insensitive to changes in correlation length for large lengths [58]. Simulations typically use a value for s in the long length range and fit the roughness amplitude alone. For example, the correlation length for the data in Figure 24 was chosen as 6 μm to bring the roughness height into an agreement with atomic force microscopy (AFM) data of similar fibers. Roughness only slightly decreases the specular reflectivity at low angles and so has almost no impact on the transmission spectra of the optics. However, roughness becomes increasingly important

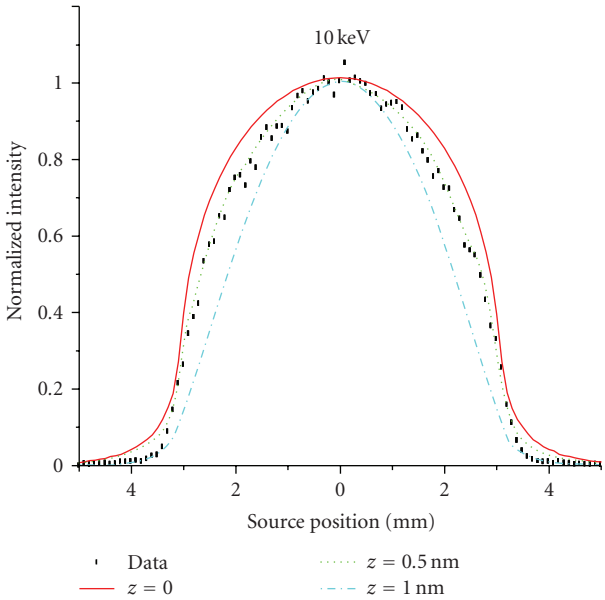

Figure 24: Roughness has little effect on the transmission of an aligned fiber, but decreases the width of the source scans in the simulation (solid colored lines) [55, 56]. For the data at 10 keV, a roughness height of 0.5 nm fits the data well.

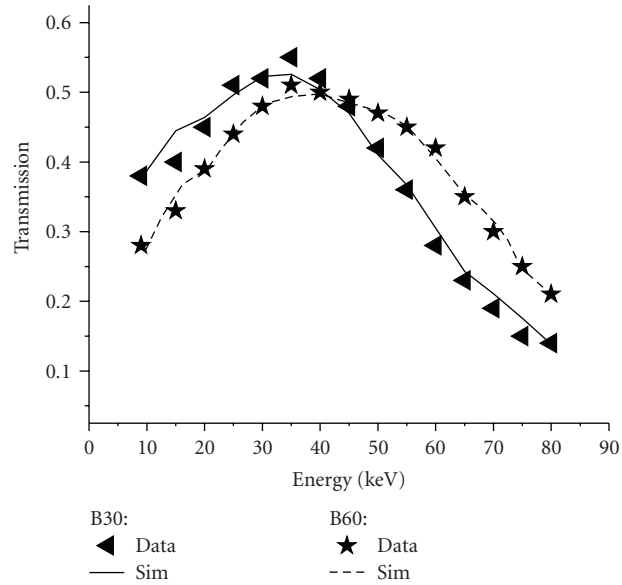

Figure 25: Transmission of two similar lead glass fibers, 30 and 60 mm in length. The simulation [55, 56] fits include 17 and 33 μm of glass layer, respectively, or 0.55 μm of blockage per mm of length [48].

under circumstances in which the angle and number of reflections increases, for example in source scans, as shown in Figure 24. Thus, it is often only necessary to include roughness in the model if the application is one for which off axis photons are important.

5.5. Absorption: Blockage and Halo. Another defect that is seen occasionally in borosilicate glass optics, and more prevalently in lead glass fibers, [47, 60] is a drop in transmission at low energies, as shown in Figure 25. Reasonable agreement is obtained over the whole range of photon energies by assuming that a layer of glass of the same composition as the channel walls blocks the channels. This glass could be dust left from the cutting process or from crystallites which have formed in the channels during drawing [61]. An increase in required layer thickness with fiber length is consistent with a stochastic random model of glass inclusions. This random probability of glass inclusions would cause the transmission to drop exponentially with optic length, as shown in Figure 26 [47]. Because of the increased processing at high temperatures, and the dust which can be induced into the channels due to the process of cutting a shaped optic, the transmission decrease at low energies is also occasionally observed for finished borosilicate optics, as shown in Figure 27.

Conversely, for a focusing optic it can be important that the halo of the unfocussed beam be removed completely by absorption in the glass walls of the optic [62]. Typically the optics are packaged in housings which contain absorptive materials, but unless care is taken in design, the focal spot may be surrounded by a "cut through" halo approximately

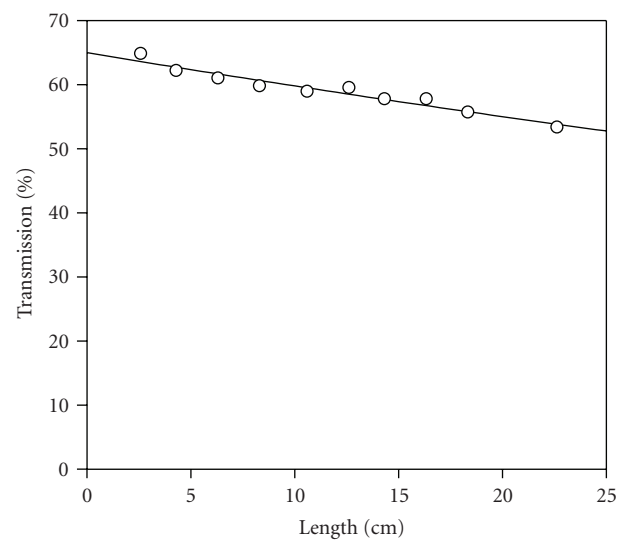

Figure 26: Measured transmission at 8 keV, as a function of length, for identical borosilicate polycapillary fibers with 17 μm channels. The solid line is an exponential fit with decay length = 120 cm.

equal to the diameter of the housing aperture [63–65]. In such cases the spot size from the optic is generally larger than predicted by (8) and does not decrease with photon energy. The expected transmission of the walls of the optic is

$$T_w = e^{-(1-f)\mu\rho x}, \tag{11}$$

where f is the fractional open area, $(1 - f)$ is the fraction filled with glass, $\mu\rho$ is the absorption coefficient of the glass, and x is the path length across the optic [66].

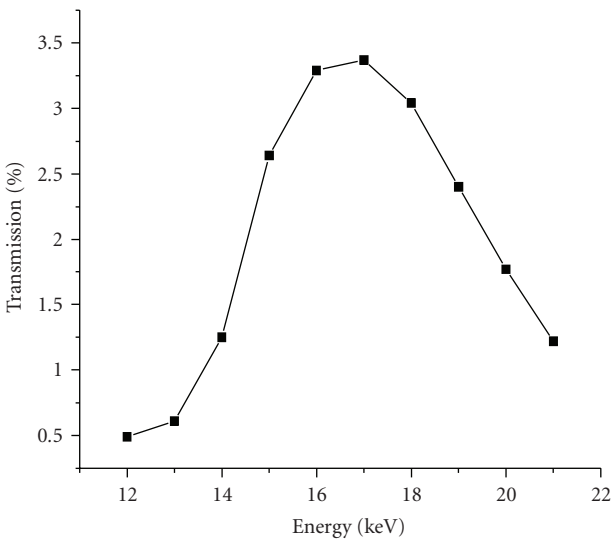

Figure 27: Drop in transmission at low energy of a sharply bent focusing polycapillary optic, possibly due to blockage by glass inclusions.

5.6. Wave Modeling and Nanocapillaries. Most simulations of polycapillary optics use simple geometric ray tracing. For coherence and wave effects to be important, the wavefront must be partially coherent over the capillary channel diameter. The transverse coherence width from a source of diameter s at a distance D for a wavelength λ is

$$L_T = \frac{\lambda}{s} D. \tag{12}$$

For a conventional source with $\lambda = 0.16\,\text{nm}$ (8 keV), $s = 200\,\mu\text{m}$, and $D = 50\,\text{mm}$, the coherence width is only about 40 nm and the typical criterion for the use of geometrical optics is well satisfied. Certain effects due to the capillary structure of the optics can still be seen in this regime [67, 68]. Coherence effects could be seen from a small part of an area of array of capillaries, even if each acts as an incoherent source, if the propagation distance is large enough to satisfy (12). For example, if two neighboring capillaries act as a source of size $s = 2d_c$, the transverse coherence of the combined source for two $5\,\mu\text{m}$ capillaries will be $100\,\mu\text{m}$ at a distance of 8 m for 10 keV X rays.

For a $5\,\mu\text{m}$ source at 1 m, the coherence width of the source is $30\,\mu\text{m}$, and interference effects might be observed between neighboring channels. To use waveguide modeling for transport down a capillary channel, the number of waveguide modes excited by the beam must be small. The number of modes is approximately [69]

$$N_{\text{modes}} = \frac{d_c}{\lambda_{\text{eff}}}, \tag{13}$$

where d_c is the diameter of a channel. For a channel size of $5\,\mu\text{m}$, and a wavelength of 0.16 nm, the number of modes is in the tens of thousands. However, this is reduced if consideration is made of the fact that only incident angles less than the critical angle are important, so the effective transverse wavelength is

$$\lambda_{\text{eff}} = \frac{\lambda}{\theta_c}. \tag{14}$$

Because both the critical angle and the wavelength increase inversely with photon energy, the effective wavelength is roughly independent of X ray photon energy and is about 40 nm. For a $5\,\mu\text{m}$ channel, this still results in hundreds of modes, but a small number of modes are present for capillaries with diameters in the submicron regime. Waveguide theory has been developed for coherent sources [69], partially coherent sources and short pulse sources [70]. Measurements for coherent sources and small channels have been performed and are consistent with wave-based calculations [71–75].

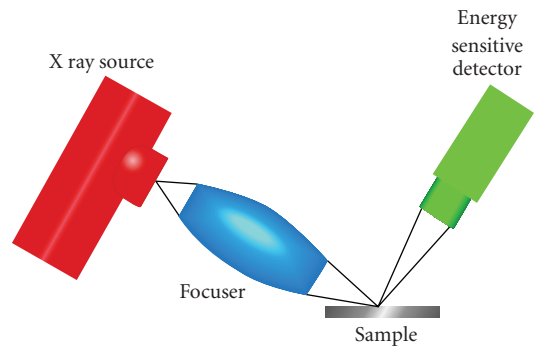

Figure 28: Geometry for XRF mapping. Courtesy of XOS.

6. Applications

6.1. X Ray Fluorescence and Spectrometry. Focusing polycapillary optics are widely used [76–79] in X ray fluorescence (XRF) and spectrometry (XRS) because of the large intensity increase compared to pinhole collimation and the resulting more flexible system design. These allow for in situ and rapid throughput systems [80, 81] as well as medical [82], and portable monitoring systems [83–85]. The smooth beam shape potentially allows for easier analysis. A large body of current work is concentrated on the issues of quantitative analysis, especially for irregularly shaped objects [86–88]. A typical geometry for conventional sources is shown in Figure 28. Rastering the sample then allows for spatial mapping. An example of the results from a volcanic inclusion is shown in Figure 29. Polycapillary focusing optics are also used on several synchrotron beam lines [39–41] for XRF, absorption spectroscopy [43], and micro XRF tomography [89, 90].

Instead of using the focusing optic on the excitation side, many groups use a focusing optic to collect the fluorescence radiation from the sample in conventional, synchrotron beam [91], proton beam [92], and particle-induced X ray emission (PIXE) [93, 94] systems.

Confocal systems such as that sketched in Figure 30 [15] provide the double benefit of enhanced signal intensity and

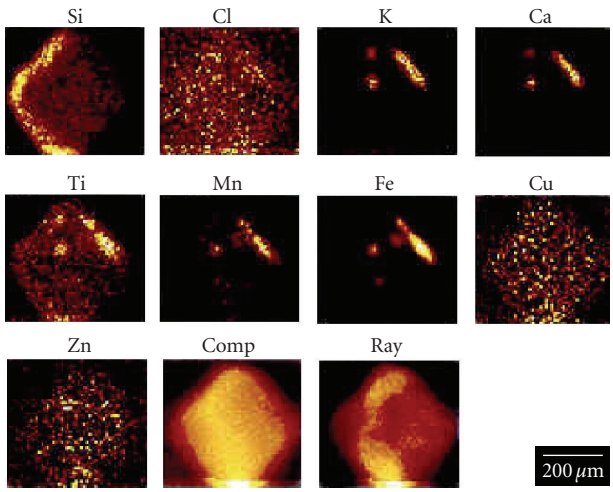

Figure 29: MXRF maps of a quartz phenocryst with small volcanic glass inclusions. Courtesy of Ning Gao, XOS.

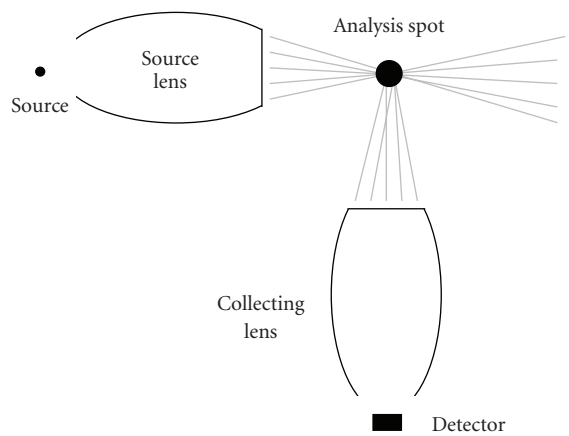

Figure 30: Sketch of microfluorescence experiment, showing that overlap of irradiation and collection volumes yield three-dimensional spatial resolution [15].

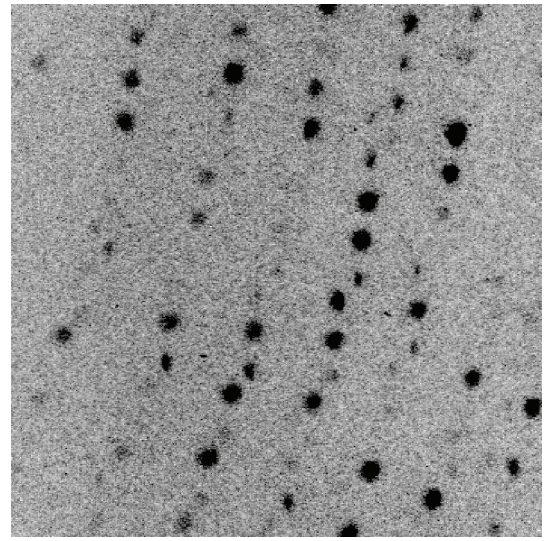

Figure 31: Lysozyme pattern taken in 20 s with 2.8 kW rotating anode, comparable to 30–35 min. without the optic. The linear R factor (a measure of the deviation from the expected intensity for all indexed reflections) was 6.4% without the optic compared to 6.9% with the optic on the same sample.

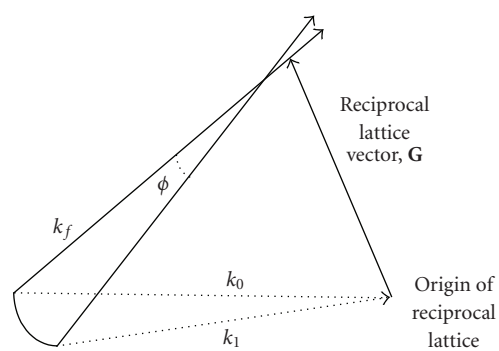

Figure 32: Ewald sphere description of focused beam diffraction on a single crystal.

three-dimensional spatial resolution. There are a growing number of confocal systems, [42, 95, 96] including multiple beam confocal systems [97].

There are also a rising number of multiple optics combinations [98], including pairing polycapillary optics with Kirkpatrick-Baez mirrors for XRF and a toroidal mirror for EXAFS [99].

6.2. Single Crystal Diffraction. Significant reduction in data collection times for single crystal diffraction can be achieved with polycapillary optics [100–103]. An image recorded in just 20 seconds is shown in Figure 31 [100]. For focused beam diffraction, the volume of reciprocal space that is accessed in a single measurement is greatly increased compared to parallel beam geometries. The local divergence from the optic, for example, 0.19° at 8 keV, is less than the ω crystal oscillations typically employed to increase the density of reflections captured in a single image in protein crystallography, so a gentle focus does not significantly broaden the spots.

Figure 32 displays a sketch of the diffraction condition for a single crystal with a monochromatic convergent beam. Diffraction conditions are satisfied for the two incident beam directions, k_0 and k_1, when they make the same angle with the reciprocal lattice vector, **G**. Thus, changing from k_0 to k_1 rotates the diffraction triangle of k_0, **G**, and k_f about the vector **G** by an angle ϕ [100]. This results in the diffracted beam, k_f, moving to trace out a tangential line on the detector as shown in Figure 33. The maximum value of ϕ is the convergence angle. There is no broadening in the transverse direction.

The effects of the one-dimensional streaking are shown in Figure 34 for a lysozyme diffraction pattern taken with a 2.1° focusing angle [103]. Serious overlap problems were not encountered except in low index directions. However, for cell dimensions >200 Å, the diffraction spots are not completely

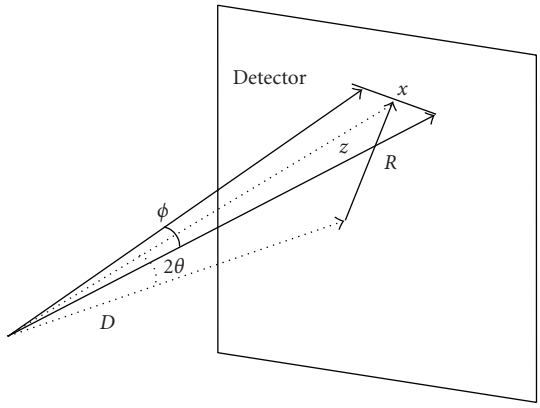

Figure 33: Diffraction streak due to beam focusing.

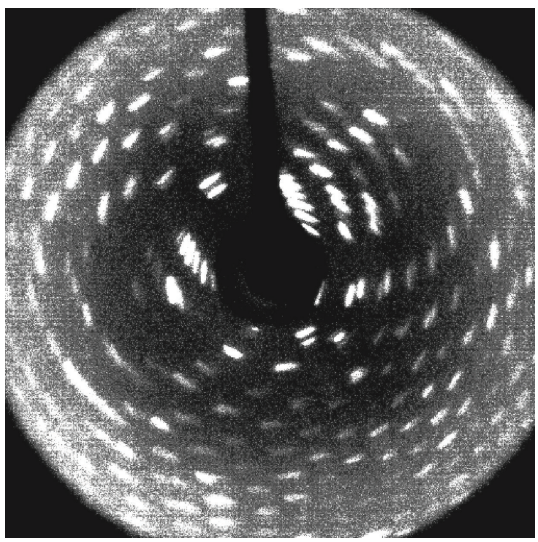

Figure 34: Lysozyme diffraction image taken in 5 minutes with a 1 mA tube source and a focusing polycapillary optic [103].

separated. Patterns with smaller convergence angles can be analyzed with conventional software and give good results [100, 104].

6.3. Powder Diffraction. Reductions in data collection time can also be obtained for powder diffraction. The symmetric beam profile and enhanced flux give improved particle and measurement statistics. While powder diffraction measurements are most commonly performed with collimating optics to reduce beam divergence, the nearly Gaussian peaks produced by the polycapillary optics provide uncertainties in peak center localization which is much less than the peak widths [33]. Thus the peak location uncertainty for powder diffraction are much smaller than the beam angle, even for highly convergent beams [36]. Polycapillary optics are also used in synchrotron systems, for example, to evaluate stresses in steel [105] and in other confocal geometries [106].

6.4. Medical Therapy and Small Animal Imaging. Polycapillary optics have been tested to provide beam shaping and

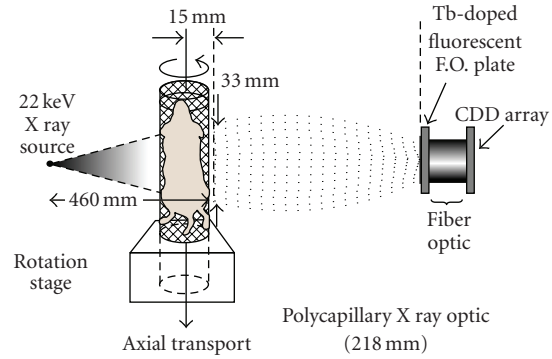

Figure 35: Focusing optic used to collect both the external beam used for computed tomography and the emission from the internal radiation emitted from the radioactively tagged pharmaceutical to produce registered images.

scatter rejection in radiography [14, 28, 47]. Beam shaping is particularly intriguing for small animal imaging. An example of a focusing optic used to collect combined computed tomography (CT) and micro Single Particle Emission CT (SPECT) images is shown in Figure 35 [107, 108]. Collecting both the external CT beam and the scintigraphy image with a single optic decreases registration error when combining scintigraphy images from a conventional γ camera with CT data.

Polycapillary optics could also be used to shape focused beams with the potential for orthovoltage therapy. Conventional X ray radiation therapy is performed with high energy X ray or gamma radiation. High-energy photons are chosen to minimize the absorbed skin dose relative to the dose at the tumor, although energies as low as 100 keV are employed in orthovoltage modalities. The choice of high energies to reduce skin dose is necessary because, in an unfocused beam, the intensity is highest near the point of entry. As an alternative method, polycapillary optics have been tested for their potential to provide a beam of lower energy X rays focused at the tumor site [109].

Neutron beams can also be focused by polycapillary optics [110–112]. A focused neutron beam could be used in boron neutron capture therapy (BNCT), based on the selective delivery of a boronated pharmaceutical to cancerous tissue followed by irradiation with thermal neutrons [113–115]. This procedure could be useful in treating near surface regions such as ocular melanomas.

6.5. Astronomy. Polycapillary optics can also be used to focus parallel beam radiation for astrophysical applications. The transmission of a 3 cm square multifiber optic developed for astrophysical applications is shown as a function of photon energy in Figure 36 [116, 117]. Polycapillary optics could be used to collect broadband radiation and redirect it to a spectroscopic detector.

6.6. Radiation Resistance. Because the X ray optical properties of materials depend on total electron density, the optical constants are insensitive to changes in electronic state.

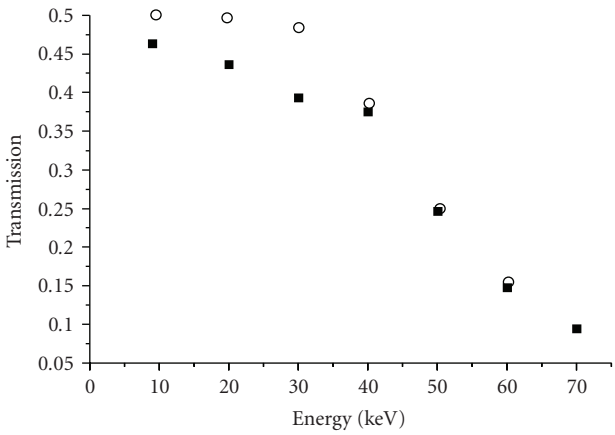

Figure 36: Simulated [116] (circles) and measured [117] (squares) transmission of a 3 cm square optic with 2 m focal length.

While color centers form rapidly in glass during exposure to intense radiation, the blackening of the glass is not indicative of a change in the X ray transmission of a polycapillary optic. Thin fibers exposed to intense beams do undergo reversible deformation due to nonuniform densification in the radiation beam. In addition, radiation-enhanced diffusion causes crystallites to grow into the channels and cause a decrease in low energy performance similar to that of Figure 27. However, rigid optics annealed *in situ* at 100 C, were shown to withstand in excess of 2 MJ/cm^2 of white beam bending magnet radiation without measurable change in performance at 8 keV [61, 118].

7. Summary

The focusing of X ray beams with polycapillary optics yields high gains in intensity and increased spatial resolution for a variety of clinical, lab-based, synchrotron, or *in situ* analysis applications. Modeling efforts accurately describe optics performance to allow for system modeling in a wide variety of geometries.

Acknowledgments

The author wishes to indicate her appreciation for data and ideas from many people, including Carmen Abreu Bittel, David Aloisi, Simon Bates, Henning Von Berlischpe, Ayhan Bingolbali, David Bittel, Cari, Dan Carter, Heather Chen, Patrick Conlon, Sonja Dittrich, Greg Downing, Sarah Formica, Christi Freinberg-Trufas, Ning Gao, David Gibson, Walter Gibson, Mikhail Gubarev, Joseph Ho, Frank Hoffman, Huapeng Huang, Huimin Hu, Abrar Hussein, Chris Jezewski, Marshall Joy, Kardiawarman, Andrei Karnaukhov, John Kimball, Ira Klotzko, David Kruger, Susanne Lee, Danhong Li, Jan Lohbreier, Dip Mahato, Kevin Matney, David Mildner, Johanna Mitchell, Charles Mistretta, Robin Moresi, Noor Mail, Scott Owens Rohrbach, Wally Peppler, Sushil Padiyar, Igor Ponomarev, Bimal Rath, Christine Russell, Robert Schmitz, Francisca Sugiro, Suparmi, Christi Trufus-Feinberg, Johannes Ullrich, Hui Wang, Lei Wang, Russel Youngman, Brian York, Qi Fan Xiao, and Wei Zhou, and for grant support from the U.S. Department of Commerce, NASA, NIH, and the Breast Cancer Research Program.

References

[1] P. B. Hirsch and J. N. Kellar, "An X ray micro-beam technique: I—collimation," *Proceedings of the Physical Society B*, vol. 64, no. 5, pp. 369–374, 1951.

[2] R. V. Pound and G. A. Rebka, "Gravitational red-shift in nuclear resonance," *Physical Review Letters*, vol. 3, no. 9, pp. 439–441, 1959.

[3] L. Marton, "X ray fiber optics," *Applied Physics Letters*, vol. 9, no. 5, pp. 194–195, 1966.

[4] P. J. Mallozzi, H. M. Epstein, R. G. Jung et al., "Laser-generated plasmas as a source of X ray for medical applications," *Journal of Applied Physics*, vol. 45, no. 4, pp. 1891–1895, 1974.

[5] W. T. Vetterling and R. V. Pound, "Measurements on an X ray light pipe at 5.9 and 14.4 keV," *Journal of the Optical Society of America*, vol. 66, no. 10, pp. 1084–1089, 1976.

[6] D. Mosher and S. J. Stephanakis, "X ray light pipes," *Applied Physics Letters*, vol. 29, no. 2, pp. 105–107, 1976.

[7] Y. M. Aleksandrov, K. A. Valiev, L. V. Velikov et al., "Transport of soft X radiation along an optical waveguide," *Soviet Technical Physics Letters*, vol. 13, no. 3, pp. 105–106, 1987.

[8] V. A. Arkad'ev, M. A. Kumakhov, and L. I. Ognev, "Total external reflection of γ rays from a surface," *Soviet Technical Physics Letters*, vol. 12, no. 11, pp. 540–542, 1986.

[9] V. A. Arkad'ev, M. A. Kumakhov, and R. F. Fayazov, "Theoretical capabilities of grazing-incidence X ray optics," *Soviet Technical Physics Letters*, vol. 14, no. 2, pp. 101–102, 1988.

[10] V. A. Arkd'ev, A. I. Kolomitsev, M. A. Kumakhov, V. V. Labuzov, and I. Y. Ponomarev, "Focusing system using multiple reflection of radiation from curved surfaces," *Soviet Technical Physics Letters*, vol. 14, no. 1, p. 42, 1988.

[11] V. A. Arkd'ev, A. I. Kolomitsev, M. A. Kumakhov et al., "Wide-band X ray optics with a large angular aperture," *Soviet Physics Uspekhi*, vol. 32, no. 3, p. 271, 1989.

[12] M. A. Kumakhov and F. F. Komarov, "Multiple reflection from surface X ray optics," *Physics Report*, vol. 191, no. 5, pp. 290–350, 1990.

[13] W. M. Gibson and C. A. MacDonald, "Polycapillary Kumakhov optics: a status report," in *X Ray and UV Detectors*, vol. 2278 of *Proceedings of SPIE*, pp. 156–167, July 1994.

[14] W. M. Gibson, C. A. MacDonald, and M. S. Kumakhov, "The Kumakhov lens; a new X ray and neutron optics with potential for medical applications," in *Technology Requirements for Biomedical Imaging*, S. K. Mun, Ed., vol. 2580, pp. 164–169, IEEE Press, New York, NY, USA, 1991.

[15] W. M. Gibson and M. A. Kumakhov, "Applications of X ray and neutron capillary optics," in *X Ray Detector Physics Applications*, vol. 1736 of *Proceedings of SPIE*, p. 172, 1992.

[16] C. A. MacDonald, C. C. Abreu, S. Budkov et al., "Quantitative measurements of the performance of capillary X ray optics," in *Multilayer and Grazing Incidence X Ray/EUV Optics II*, R. B. Hoover and A. Walker, Eds., vol. 2011 of *Proceedings of SPIE*, pp. 275–286, 1993.

[17] J. B. Ullrich, V. Kovantsev, and C. A. MacDonald, "Measurements of polycapillary X ray optics," *Journal of Applied Physics*, vol. 74, no. 10, pp. 5933–5939, 1993.

[18] B. Rath, R Youngman, and C. A. MacDonald, "An automated test system for measuring polycapillary X ray optics," *Review of Scientific Instrumentation*, vol. 65, pp. 3393–3398, 1994.

[19] J. B. Ullrich, I. Y. Ponomarev, M. V. Gubarev, N. Gao, Q. F. Xiao, and W. M. Gibson, "Development of monolithic capillary optics for X ray diffraction applications," in *X Ray and UV Detectors*, R. B. Hoover and R. B. Tate, Eds., vol. 2278 of *Proceedings of SPIE*, pp. 148–155, 1994.

[20] C. A. Macdonald, "Applications and measurements of polycapillary X ray optics," *Journal of X Ray Science and Technology*, vol. 6, no. 1, pp. 32–47, 1996.

[21] C. C. Abreu and C. A. MacDonald, "Beam collimation, focusing, filtering and imaging with polycapillary X ray and neutron optics," *Physica Medica*, vol. 13, no. 3, pp. 79–89, 1997.

[22] V. A. Arkadiev and D. I. Gruev, "Principal possibilities of Kumakhov lenses," in *X Ray and UV Detectors*, vol. 2278 of *Proceedings of SPIE*, pp. 200–209, July 1994.

[23] M. A. Kumakhov, "Status of X ray capillary optics," in *X Ray and Extreme Ultraviolet Optics*, R. B. Hoover and A. B. C. Walker Jr., Eds., vol. 2515 of *Proceedings of SPIE*, pp. 86–102, 1995.

[24] V. A. Arkadiev, A. A. Bzhaumikhov, H. E. Gorny, and N. S. Ibraimov, "Experimental investigation of Kumakhov lenses," in *X Ray and Extreme Ultraviolet Optics*, R. B. Hoover and A. B. C. Walker Jr., Eds., vol. 2515 of *Proceedings of SPIE*, pp. 103–113, 1995.

[25] M. A. Kumakhov, "Development of X ray and neutron capillary optics," in *Grazing Incidence and Multilayer X Ray Optical Systems*, R. B. Hoover and A. B. C. Walker Jr., Eds., vol. 3113 of *Proceedings of SPIE*, pp. 362–368, 1997.

[26] M. A. Kumakhov, "X ray capillary optics: history of development and present status," in *Kumakhov Optics and Application: Selected Research Papers on Kumakhov Optics and Application of 1998–2000*, M. A. Kumakhov, Ed., vol. 4155 of *Proceedings of SPIE*, pp. 2–12, 2000.

[27] C. A. MacDonald and W. M. Gibson, "Polycapillary optics," in *Handbook of Optics*, M. Bass, C. DeCusatis, J. Enoch et al., Eds., vol. 5 of *Atmospheric Optics, Modulators, Fiber Optics, X Ray and Neutron Optics*, McGraw-Hill, New York, NY, USA, 3rd edition, 2010.

[28] G. Cappuccio and S. B. Dabagov, "Capillary optics as an X ray condensing lens: an alignment procedure," in *Kumakhov Optics and Application: Selected Research Papers on Kumakhov Optics and Application 1998–2000*, M. A. Kumakhov, Ed., vol. 4155 of *Proceedings of SPIE*, pp. 40–47, 2000.

[29] D. Li, F. R. Sugiro, and C. A. MacDonald, "Source-optic optimization for compact monochromatic imaging," in *X Ray Sources and Optics*, C. A. MacDonald, A. T. Macrander, T. Ishikawa, C. Morawe, and J. L. Woo, Eds., vol. 5537 of *Proceedings of SPIE*, pp. 105–114, 2004.

[30] T. Sun and X. Ding, "Study on the measurement of properties of polycapillary X ray lens," *Nuclear Instruments and Methods*, vol. 226, no. 4, pp. 651–658, 2004.

[31] A. Bingölbali and C. A. MacDonald, "Quality assessment system for curved crystal X ray optics," *Nuclear Instruments and Methods*, vol. 267, no. 5, pp. 832–841, 2009.

[32] S. M. Owens, J. B. Ullrich, I. Y. Ponomarev et al., "Polycapillary X ray optics for macromolecular crystallography," in *Hard X Ray/Gamma-Ray and Neutron Optics, Sensors, and Applications*, R. B. Hoover and F. B. Doty, Eds., vol. 2859, pp. 200–209, 1996.

[33] W. Zhou, D. N. Mahato, and C. A. MacDonald, "Analysis of powder X ray diffraction resolution using collimating and focusing polycapillary optics," *Thin Solid Films*, vol. 518, no. 18, pp. 5047–5056, 2010.

[34] R. E. Ban Gridken and A. A. Markowicz, *Handbook of X Ray Spectrometry*, Marcel Dekker, New York, NY, USA, 1993.

[35] A. Thompson, D. Atlword, E. Gullikson et al., *X Ray Data Booklet*, CXRO, Berkeley, Calif, USA, 2002.

[36] A. Bingölbali, W. Zhou, D. N. Mahato, and C. A. MacDonald, "Focused beam powder diffraction with polycapillary and curved crystal optics," in *Advances in X Ray/EUV Optics and Components III*, A. M. Khounsary, C. Morawe, and S. Goto, Eds., vol. 7077 of *Proceedings of SPIE*, 2008.

[37] F. A. Hoffman, N. Gao, S. M. Owens, W. M. Gibson, C. A. MacDonald, and S. M. Lee, "Polycapillary optics for in-situ process diagnotstics," in *In Situ Process Diagnostics and Intelligent Materials Processing, Materials Research Society Proceedings*, P. A. Rosenthal, W. M. Duncan, and J. A. Woollam, Eds., vol. 502, pp. 133–138, 1998.

[38] F. A. Hofmann, C. A. Freinberg-Trufas, S. M. Owens, S. D. Padiyar, and C. A. MacDonald, "Focusing of synchrotron radiation with polycapillary optics," *Nuclear Instruments and Methods*, vol. 133, no. 1-4, pp. 145–150, 1997.

[39] A. Erko, F. Schäfers, A. Firsov, W. B. Peatman, W. Eberhardt, and R. Signorato, "The BESSY X ray microfocus beamline project," *Spectrochimica Acta B*, vol. 59, no. 10-11, pp. 1543–1548, 2004.

[40] A. Al-Ebraheem, A. Mersov, K. Gurusamy, and M. J. Farquharson, "Distribution of Ca, Fe, Cu and Zn in primary colorectal cancer and secondary colorectal liver metastases," *Nuclear Instruments and Methods A*, vol. 619, no. 1–3, pp. 338–343, 2010.

[41] V. G. Mihucz, G. Silversmit, I. Szalóki et al., "Removal of some elements from washed and cooked rice studied by inductively coupled plasma mass spectrometry and synchrotron based confocal micro-X ray fluorescence," *Food Chemistry*, vol. 121, no. 1, pp. 290–297, 2010.

[42] K. Janssens, K. Proost, and G. Falkenberg, "Confocal microscopic X ray fluorescence at the HASYLAB microfocus beamline: characteristics and possibilities," *Spectrochimica Acta B*, vol. 59, no. 10-11, pp. 1637–1645, 2004.

[43] G. Silversmit, B. Vekemans, S. Nikitenko et al., "Polycaillary based μ-XAS and confocal μ-XANES at a bending magnet source of the ESRF," *Journal of Physics: Conference Series*, vol. 190, Article ID 012036, 2009.

[44] A. Erko, N. Langhoff, A. A. Bjeoumikhov, and V. I. Beloglasov, "High-order harmonic suppression by a glass capillary array," *Nuclear Instruments and Methods*, vol. 467-468, pp. 832–835, 2001.

[45] V. Rossi Albertini, B. Paci, A. Generosi, S. B. Dabagov, O. Mikhin, and M. A. Kumakhov, "On the use of polycapillary structures to improve laboratory Energy-Dispersive X ray Diffractometry and Reflectometry," *Spectrochimica Acta B*, vol. 62, no. 11, pp. 1203–1207, 2007.

[46] Q. F. Xiao, I. Y. Ponomarev, A. I. Kolomitsev, and J. C. Kimball, "Numerical simulations for capillary-based X ray optics," in *X Ray Detector Physics and Applications*, R. B. Hoover, Ed., Proceedings of SPIE, 1992.

[47] C. C. Abreu, D. G. Kruger, C. A. MacDonald, C. A. Mistretta, W. W. Peppler, and Q. F. Xiao, "Measurements of capillary X ray optics with potential for use in mammographic imaging," *Medical Physics*, vol. 22, no. 11, part 1, pp. 1793–1801, 1995.

[48] Suparmi, Cari, L. Wang, H. Wang, W. M. Gibson, and C. A. MacDonald, "Measurement and analysis of leaded glass capillary optic performance for hard X ray applications," *Journal of Applied Physics*, vol. 90, no. 10, pp. 5363–5368, 2001.

[49] C. A. MacDonald and W. M. Gibson, "Applications and advances in polycapillary optics," *X Ray Spectrometry*, vol. 32, no. 3, pp. 258–268, 2003.

[50] A. Liu, "The X ray distribution after a focussing polycapillary—a shadow simulation," *Nuclear Instruments and Methods B*, vol. 243, no. 1, pp. 223–226, 2006.

[51] D. Hampai, G. Cappuccio, G. Cibin, S. B. Dabagov, and V. Sessa, "Modeling of X ray transport through polycapillary optics," *Nuclear Instruments and Methods A*, vol. 580, no. 1, pp. 85–89, 2007.

[52] D. Hampai, S. B. Dabagov, G. Cappuccio, and G. Cibin, "X ray propagation through polycapillary optics studied through a ray tracing approach," *Spectrochimica Acta B*, vol. 62, no. 6-7, pp. 608–614, 2007.

[53] L. Xiaoyan, LI. Yude, T. Guotai, and S. Tianxi, "Evaluation of transmitting performance of cylindrical polycapillary," *Nuclear Instruments and Methods*, vol. 572, no. 2, pp. 729–733, 2007.

[54] F. R. Sugiro, S. D. Padiyar, C. A. MacDonald, and C. A. MacDonald, "Characterization of pre- and post-patient X ray polycapillary optics for mammographic imaging," in *Advances in Laboratory-Based X Ray Sources and Optics*, R. B. Hoover, A. B. C. Walker II, and S. Goto, Eds., vol. 4144 of *Proceedings of SPIE*, pp. 204–215, 2000.

[55] L. Wang, B. K. Rath, W. M. Gibson, J. C. Kimball, and C. A. MacDonald, "Performance study of polycapillary optics for hard X rays," *Journal of Applied Physics*, vol. 80, no. 7, pp. 3628–3638, 1996.

[56] H. Wang, L. Wang, W. M. Gibson, and C. A. MacDonald, "Focused beam powder diffraction with polycapillary and curved crystal optics," in *X Ray Optics, Instruments, and Missions*, R. B. Hoover, A. B. C. Walker II, and S. Goto, Eds., vol. 3444 of *Proceedings of SPIE*, pp. 643–651, July 1998.

[57] D. H. Bilderback, "Review of capillary X ray optics from the 2nd international capillary optics meeting," *X Ray Spectrometry*, vol. 32, no. 3, pp. 195–207, 2003.

[58] D. Bittel and J. C. Kimball, "Surface roughness and the scattering of glancing-angle X rays: application to X ray lenses," *Journal of Applied Physics*, vol. 74, no. 2, pp. 877–883, 1993.

[59] J. Harvey, "X ray optics," in *Handbook of Optics*, M. Bass, Ed., vol. 2, chapter 11, McGraw-Hill, New York, NY, USA, 1st edition, 1996.

[60] Cari, C. A. MacDonald, W. M. Gibson et al., "Characterization of a long focal length polycapillary optic for high energy X rays," in *Advances in Laboratory-Based X Ray Sources and Optics*, C. A. MacDonald and A. M. Khounsary, Eds., vol. 4144 of *Proceedings of SPIE*, pp. 183–192, 2000.

[61] B. K. Rath, L. Wang, B. E. Homan, F. Hofmann, W. M. Gibson, and C. A. MacDonald, "Measurements and analysis of radiation effects in polycapillary X ray optics," *Journal of Applied Physics*, vol. 83, no. 12, pp. 7424–7435, 1998.

[62] A. Bjeoumikhov, N. Langhoff, S. Bjeoumikhova, and R. Wedell, "Capillary optics for micro X ray fluorescence analysis," *Review of Scientific Instruments*, vol. 76, no. 6, Article ID 063115, 2005.

[63] S. Dittrich, *Energy sensitive measurements of X Ray beam focusing with polycapillary optics*, M.S. thesis, University at Albany, 2006.

[64] H. von Berlischpe, *Focused beam applications polycapillary X ray optics*, M.S. thesis, University at Albany, 2005.

[65] J. Lohbreier, *Fluorescence and diffraction measurements with polycapillary X ray optics*, M.S. thesis, University at Albany, 2004.

[66] L. Wang, W. M. Gibson, C. A. MacDonald et al., "Potential of polycapillary X ray optics in medical imaging applications," in *EUV, X Ray, and Neutron Optics and Sources*, C. A. MacDonald, K. A. Goldberg, J. R. Maldonado, A. J. Marker III, and S. P. Vernon, Eds., vol. 3767 of *Proceedings of SPIE*, pp. 102–112, 1999.

[67] M. A. Kumakhov, "Status of experimental works in the field of X ray capillary optics," in *X Ray and UV Detectors*, vol. 2278 of *Proceedings of SPIE*, pp. 180–190, July 1994.

[68] S. B. Dabagov, A. Marcelli, V. A. Murashova, N. L. Svyatoslavsky, R. V. Fedorchuk, and M. N. Yakimenko, "Coherent and incoherent components of a synchrotron radiation spot produced by separate capillaries," *Applied Optics*, vol. 39, no. 19, pp. 3338–3343, 2000.

[69] S. B. Dabagov and H. Uberall, "On X ray channeling in narrow guides," *Nuclear Instruments and Methods*, vol. 266, no. 17, pp. 3881–3887, 2008.

[70] S. V. Kukhlevsky, G. Nyitray, V. L. Kantsyrev, and J. Kaiser, "Detailed structure of fs pulses passing through straight and tapered optical waveguides," *Optics Communications*, vol. 192, no. 3–6, pp. 225–229, 2001.

[71] S. LaBrake, *Glass capillary X ray waveguides*, Doctoral Dissertation, University at Albany, 2003.

[72] A. Bjeoumikhov, S. Bjeoumikhova, H. Riesemeier, M. Radtke, and R. Wedell, "Propagation of synchrotron radiation through nanocapillary structures," *Physics Letters A*, vol. 366, no. 4-5, pp. 283–288, 2007.

[73] S. V. Kukhlevsky, F. Flora, A. Marinai et al., "Diffraction of X ray beams in capillary waveguides," *Nuclear Instruments and Methods B*, vol. 168, no. 2, pp. 276–282, 2000.

[74] A. Bjeoumikhov, "Observation of peculiarities in angular distributions of X ray radition after propagation through nanocapill structure," *Physics Letters A*, vol. 360, pp. 405–410, 2007.

[75] S. B. Dabagov, "Channeling of neutral particles in micro- and nanocapillaries," *Physics-Uspekhi*, vol. 46, no. 10, pp. 1053–1075, 2003.

[76] K. Janssens, W. De Nolf, G. Van Der Snickt et al., "Recent trends in quantitative aspects of microscopic X ray fluorescence analysis," *Trends in Analytical Chemistry*, vol. 29, no. 6, pp. 464–478, 2010.

[77] K. Tsuji, K. Nakano, H. Hayashi, K. Hayashi, and C. U. Ro, "X ray spectrometry," *Analytical Chemistry*, vol. 80, no. 12, pp. 4421–4454, 2008.

[78] K. H. A. Janssens, F. C. V. Adams, and A. Rindby, Eds., *Microscopic X Ray Fluorescence Analysis*, John Wiley & Sons, New York, NY, USA, 2000.

[79] Y. Yan and W. M. Gibson, "Polycapillary optics and X ray analytical techniques," *Advances in X Ray Analysis*, vol. 45, pp. 298–304, 2002.

[80] S. P. Formica and S. M. Lee, "X ray fluorescence system for thin film composition analysis during deposition," *Thin Solid Films*, vol. 491, no. 1-2, pp. 71–77, 2005.

[81] Z. Luo, B. Geng, J. Bao et al., "High-throughput X ray characterization system for combinatorial materials studies," *Review of Scientific Instruments*, vol. 76, no. 9, Article ID 095105, 2005.

[82] L. Borgese, A. Zacco, E. Bontempi et al., "Use of total reflection X ray fluorescence (TXRF) for the evaluation of heavy metal poisoning due to the improper use of a traditional ayurvedic drug," *Journal of Pharmaceutical and Biomedical Analysis*, vol. 52, no. 5, pp. 787–790, 2010.

[83] S. V. Nikitina, A. S. Shcherbakov, and N. S. Ibraimov, "X ray fluorescence analysis on the base of polycapillary Kumakhov optics," *Review of Scientific Instruments*, vol. 70, no. 7, pp. 2950–2956, 1999.

[84] G. Buzanich, P. Wobrauschek, C. Streli et al., "A portable micro-X ray fluorescence spectrometer with polycapillary optics and vacuum chamber for archaeometric and other applications," *Spectrochimica Acta B*, vol. 62, no. 11, pp. 1252–1256, 2007.

[85] G. Vittiglio, S. Bichlmeier, P. Klinger et al., "A compact μ-XRF spectrometer for (in situ) analyses of cultural heritage and forensic materials," *Nuclear Instruments and Methods B*, vol. 213, pp. 693–698, 2004, 5th Topical Meeting on Industrial Radiation andRadioisotope Measurement Applications.

[86] B. Kanngießer, N. Kemf, and W. Malzer, "Spectral and lateral resolved characterisation of X ray microbeams," *Nuclear Instruments and Methods B*, vol. 198, no. 3-4, pp. 230–237, 2002.

[87] E. Langer, S. Dabritz, W. Hauffe, and M. Haschke, "Advances in X ray excitation of Kossel patterns by a focusing polycapillary lens," *Applied Surface Science*, vol. 252, no. 1, pp. 240–244, 2005.

[88] A. G. Revenko, "Specific features of X ray fluorescence analysis techniques using capillary lenses and synchrotron radiation," *Spectrochimica Acta B*, vol. 62, no. 6-7, pp. 567–576, 2007.

[89] J. M. Feldkamp, C. G. Schroer, J. Patommel et al., "Compact X ray microtomography system for element mapping and absorption imaging," *Review of Scientific Instruments*, vol. 78, no. 7, Article ID 073702, 2007.

[90] P. Bleuet, P. Gergaud, L. Lemelle et al., "3D chemical imaging based on a third-generation synchrotron source," *Trends in Analytical Chemistry*, vol. 29, no. 6, pp. 518–527, 2010.

[91] Ž. Šmit, K. Janssens, K. Proost, and I. Langus, "Confocal μ-XRF depth analysis of paint layers," *Nuclear Instruments and Methods B*, vol. 219-220, no. 1–4, pp. 35–40, 2004.

[92] M. Žitnik, P. Pelicon, N. Grlj et al., "Three-dimensional imaging of aerosol particles with scanning proton microprobe in a confocal arrangement," *Applied Physics Letters*, vol. 93, no. 9, Article ID 094104, 2008.

[93] N. Grassi, C. Guazzoni, R. Alberti, T. Klatka, and A. Bjeoumikhov, "External scanning micro-PIXE for the characterization of a polycapillary lens: measurement of the collected X ray intensity distribution," *Nuclear Instruments and Methods B*, vol. 268, no. 11-12, pp. 1945–1948, 2010.

[94] R. Alberti, A. Bjeoumikhov, N. Grassi et al., "Use of silicon drift detectors for the detection of medium-light elements in PIXE," *Nuclear Instruments and Methods B*, vol. 266, no. 10, pp. 2296–2300, 2008.

[95] T. Sun, Z. Liu, Y. Li et al., "Quantitative analysis of single aerosl particles with confocal micro-X ray fluorescence spectrometer," *Nuclear Instruments and Methods A*, vol. 622, no. 1, pp. 295–297, 2010.

[96] A. Castoldi, C. Guazzoni, R. Hartmann, C. Ozkan, L. Strüder, and A. Visconti, "Application of controlled-drift detectors to spectroscopic X ray imaging," in *Proceedings of the IEEE Nuclear Science Symposium and Medical Imaging Conference (NSS-MIC '07)*, pp. 1003–1008, November 2007.

[97] K. Tsuji, K. Nakano, and X. Ding, "Development of confocal micro X ray fluorescence instrument using two X ray beams," *Spectrochimica Acta B*, vol. 62, no. 6-7, pp. 549–553, 2007.

[98] W. M. Gibson and C. A. MacDonald, "Summary of X ray and neutron optics," in *Handbook of Optics*, M. Bass, Ed., vol. 3, chapter 37, McGraw-Hill, New York, NY, USA, 2000.

[99] T. Sun, Y. Xie, Z. Liu, T. Liu, T. Hu, and X. Ding, "Application of a combined system of polycapillary X ray lens and toroidal mirror in micro-X ray-absorption fine-structure facility," *Journal of Applied Physics*, vol. 99, no. 9, Article ID 094907, 2006.

[100] P.-W. Li and R.-C. Bi, "Applications of polycapillary X ray optics in protein crystallography," *Journal of Applied Crystallography*, vol. 31, no. 5, pp. 806–811, 1998.

[101] F. A. Hofmann, W. M. Gibson, C. A. MacDonald, D. A. Carter, J. X. Ho, and J. R. Ruble, "Polycapillary optic-source combinations for protein crystallography," *Journal of Applied Crystallography*, vol. 34, no. 3, pp. 330–335, 2001.

[102] C. A. MacDonald, S. M. Owens, and W. M. Gibson, "Polycapillary X ray optics for microdiffraction," *Journal of Applied Crystallography*, vol. 32, no. 2, pp. 160–167, 1999.

[103] S. M.. Owens, F. A. Hoffman, C. A. MacDonald, and W. M. Gibson, "Microdiffraction using collimating and convergent beam polycapillary optics," *Advances in X Ray Analysis*, vol. 41, pp. 314–318, 1997.

[104] J. X. Ho, E. H. Snell, R. C. Sisk et al., "Stationary crystal diffraction with a monochromatic convergent X ray source and application for macromolecular crystal data collection," *Acta Crystallographica D*, vol. 54, no. 2, pp. 200–214, 1998.

[105] C. Kirchlechner, K. J. Martinschitz, R. Daniel et al., "X ray diffraction analysis of three-dimensional residual stress fields reveals origins of thermal fatigue in uncoated and coated steel," *Scripta Materialia*, vol. 62, no. 10, pp. 774–777, 2010.

[106] S. T. Misture and M. Haller, "Application of polycapillary optics for parallel beam powder diffraction," *Advances in X Ray Analysis*, vol. 43, pp. 248–253, 2000.

[107] C. A. MacDonald, N. Mail, W. M. Gibson, S. M. Jorgensen, and E. L. Ritman, "Micro gamma camera optics with high sensitivity and resolution," in *Physics of Medical Imaging*, M. J. Flynn, Ed., vol. 5745 of *Proceedings of SPIE*, pp. 1–6, 2005.

[108] S. M. Jorgensen, M. S. Chmelik, D. R. Eaker, C. A. MacDonald, and E. L. Ritman, "Polycapillary X ray optics- based integrated micro-SPECT/CT scanner," in *Developments in X Ray Tomography IV*, U. Bonse, Ed., vol. 5535 of *Proceedings of SPIE*, pp. 36–42, 2004.

[109] D. N. Mahato and C. A. MacDonald, "Potential for focused beam orthovoltage therapy," in *Penetrating Radiation Systems and Applications XI*, F. P. Doty, H. B. Barber, H. Roehrig, and R. C. Schirato, Eds., vol. 7806 of *Proceedings of SPIE*, 2010.

[110] H. Chen, R. G. Downing, D. F. R. Mildner et al., "Guiding and focusing neutron beams using capillary optics," *Nature*, vol. 357, no. 6377, pp. 391–393, 1992.

[111] Q. F. Xiao, H. Chen, V. A. Sharov et al., "Neutron focusing optic for submillimeter materials analysis," *Review of Scientific Instruments*, vol. 65, no. 11, pp. 3399–3402, 1994.

[112] D. F. R. Mildner, H. H. Chen-Mayer, and R. G. Downing, "Characteristic of a polycapillary neutron focusing lens," in *Proceedings of the International Symposium on Advanced in Neutron Optics and Related Research Facilities*, Japan, March 1996.

[113] R. F. Barth, A. H. Soloway, and R. G. Fairchild, "Boron neutron capture therapy for cancer," *Scientific American*, vol. 263, no. 4, pp. 100–106, 1990.

[114] A. J. Peurrung, "Capillary optics for neutron capture therapy," *Medical Physics*, vol. 23, no. 4, pp. 487–494, 1996.

[115] R. Mayer, J. Welsh, and H. Chen-Mayer, "Focused neutron beam dose deposition profiles in tissue equivalent materials: a pilot study of BNCT," in *Proceedings of the 5th International Conference on Neutron Techniques*, Crete, Greece, June 1996.

[116] C. H. Russell, W. M. Gibson, M. V. Gubarev et al., "Application of polycapillary optics for hard X ray astronomy," in *Grazing Incidence and Multilayer X Ray Optical Systems*, R. B. Hoover and A. B. C. Walker II, Eds., vol. 3113 of *Proceedings of SPIE*, pp. 369–377, 1997.

[117] C. H. Russell, M. Gubarev, J. Kolodziejczak, M. Joy, C. A. MacDonald, and W. M. Gibson, "Polycapillary X ray optics for X ray Astronomy," in *Advances in X Ray Analysis*, vol. 43, 1999.

[118] B. K. Rath, F. B. Hagelberg, B. E. Homan, and C. A. MacDonald, "Synchrotron white beam thermal loading on polycapillary X ray optics," *Nuclear Instruments and Methods*, vol. 401, no. 2-3, pp. 421–428, 1997.